Band-edge hole mass in strained-quantum-well structures

Ikuo Suemune
Faculty of Engineering, Hiroshima University, Shitami, Saijocho, Higashihiroshima 724, Japan
(Received 14 August 1990; revised manuscript received 17 January 1991)

An analytical expression for the hole mass at the top of the valence band was derived for a strained quantum well (QW) grown on a (001) substrate assuming infinite barriers. This expression for the hole mass indicates that the mass value is isotropic in the (001) QW plane even if the warping of the valence band is taken into account. The mass values estimated from this analytical expression were compared with those calculated numerically by treating the boundary conditions exactly at the heterointerface, and the effects of the finite-barrier height and the strain were studied. The comparison of the calculated mass values with the measurements was also discussed.

I. INTRODUCTION

Strain in semiconductor quantum-well (QW) structures is known to modify the band structures.[1] The valence-band structure near the zone center is significantly reshaped with strain, and the biaxial compression in the QW plane improves the lasing properties in semiconductor QW's due to the reduced density of states in the valence band.[2–5] These laser characteristics are usually analyzed using material parameters, such as the effective masses of the respective band. However, the study of the band structures in strained QW's up to now has been mainly based on numerical calculations, and this has made the device characterizations rather difficult.

In this paper, an analytical expression of the hole mass at the top of the valence band was derived for strained QW's grown on (001) substrates. The expression was derived assuming the infinite-barrier height and the validity of the model was examined by comparing it with the numerical calculations of the band structure, taking into account the finite-barrier height. In Sec. II, the analysis based on the Luttinger-Kohn (LK) formalism[6] is given, which takes into account the finite-barrier height. In Sec. III, the analytical expression for the band-edge hole mass is derived by simplifying the analytical procedure given in Sec. II assuming the infinite-barrier height. The derived hole mass is shown to be isotropic in the (001) QW plane. In Sec. IV, the strain dependence of the band-edge hole mass and the effect of the finite-barrier height are discussed for $In_xGa_{1-x}As$ alloy strained QW's, and a comparison with the available measured mass values will be discussed. In Sec. V, some additional discussions on the validity of the approximations used in the preceding sections are given. Finally, in Sec. VI the main results in this paper are summarized.

II. THEORETICAL TREATMENT OF VALENCE-BAND STRUCTURE

The total Hamiltonian which describes the band structure of the strained QW is given by

$$H = H_0 + H_s \ , \tag{1}$$

where H_0 and H_s are the LK Hamiltonian and the strain Hamiltonian, respectively. In the LK formalism for H_0, where a canonical transform is used to eliminate the first-order term and is accurate to second order, the conduction band is decoupled.[6] Eppenga, Schuurmans, and Colak[7] included additional first-order terms to take the coupling of the conduction band and the other valence bands into account. In their method, eight bands which result in an 8×8 Hamiltonian matrix were treated simultaneously.

In the strained QW's under biaxial compression, which are mainly treated below, the valence-band edge is given by the band designated by $|J,m_J\rangle = |\frac{3}{2},\pm\frac{3}{2}\rangle$. This band corresponds to the bulk heavy-hole (HH) band without strain, but frequently it is called the light-hole (LH) band since the in-plane hole mass becomes smaller. In this paper, the $|\frac{3}{2},\pm\frac{3}{2}\rangle$ band will be called the HH band following the naming in the conventional bulk band structure.

The fundamental property of this HH band may become clearer by surveying the related theoretical results reported up to now. In the $\mathbf{k}\cdot\mathbf{p}$ method, the HH band remains uncoupled to the other bands in the first-order formalism.[8] This indicates that the HH band is very weakly coupled to the conduction (C) band and the spin-orbit split-off (SO) band near the zone center, which are separated in energy from the band edge of the HH band. This is evidenced by the reported numerical results in the following. Chitta, Degani, and Cohen treated the 6×6 Hamiltonian, which included the C, HH, and LH bands.[9] The modification of the lowest HH subband dispersion in a $GaAs/Al_xGa_{1-x}As$ QW by the inclusion of the coupling between the conduction band and the valence band was very small. Citrin and Chang calculated the valence-band dispersion for GaAs quantum wires considering the coupling of the HH, LH, and SO bands.[10] Their results indicated that the lowest HH subband near the zone center remained almost unaffected with the inclusion of the coupling to the SO band. The other subbands were affected a little more by taking this coupling into account.

Under the above situation, the reduction of the matrix size becomes possible with good accuracy when the study

is mainly aimed at the characterization of the lowest HH subband near the zone center. When the coupling of the HH band to the C and SO bands is neglected, the LK Hamiltonian is reduced to the following 4×4 matrix:

$$\begin{bmatrix} F & L & M & 0 \\ L^* & G & 0 & M \\ M^* & 0 & G & -L \\ 0 & M^* & -L^* & F \end{bmatrix}, \tag{2}$$

where

$$\begin{aligned} F&=-\frac{\hbar^2}{2m_0}[(\gamma_1+\gamma_2)k_t^2+(\gamma_1-2\gamma_2)k_z^2] , \\ G&=-\frac{\hbar^2}{2m_0}[(\gamma_1-\gamma_2)k_t^2+(\gamma_1+2\gamma_2)k_z^2] , \\ L&=\frac{\hbar^2}{2m_0}[2\sqrt{3}\gamma_3(k_x-ik_y)k_z] , \\ M&=\frac{\hbar^2}{2m_0}[\sqrt{3}\gamma_2(k_x^2-k_y^2)-i2\sqrt{3}\gamma_3k_xk_y] . \end{aligned} \tag{3}$$

γ_1, γ_2, and γ_3 are the Luttinger mass parameters, and $k_t^2=k_x^2+k_y^2$. The corresponding basis set is given by

$$\begin{aligned} |u_1\rangle&=|\tfrac{3}{2},\tfrac{3}{2}\rangle=|-(1/\sqrt{2})(X+iY)\uparrow\rangle , \\ |u_2\rangle&=|\tfrac{3}{2},\tfrac{1}{2}\rangle=|(1/\sqrt{6})[-(X+iY)\downarrow+2Z\uparrow]\rangle , \\ |u_3\rangle&=|\tfrac{3}{2},-\tfrac{1}{2}\rangle=|(1/\sqrt{6})[(X-iY)\uparrow+2Z\downarrow]\rangle , \\ |u_4\rangle&=|\tfrac{3}{2},-\tfrac{3}{2}\rangle=|(1/\sqrt{2})(X-iY)\downarrow\rangle . \end{aligned} \tag{4}$$

When a QW is under biaxial strain in the (001) QW plane, the components of the strain are given by

$$\begin{aligned} \epsilon_{xx}&=\epsilon_{yy}\equiv\epsilon_{\parallel}=\frac{\Delta a}{a} , \\ \epsilon_{zz}&=-\frac{2C_{12}}{C_{11}}\epsilon_{\parallel} , \\ \epsilon_{xy}&=\epsilon_{yx}=\epsilon_{zx}=0 , \end{aligned} \tag{5}$$

where $\Delta a/a$ is the strain due to the lattice mismatch at the heterointerface and C_{11} and C_{12} are the stiffness constants. The (001) QW plane was assumed to be the x-y coordinate plane in the present treatment. Under this circumstance, the strain Hamiltonian[11] H_s is reduced to

$$H_s=-E_H-\frac{3}{\hbar^2}E_U(\mathbf{L}_z^2-\tfrac{1}{3}\mathbf{L}^2) , \tag{6}$$

where

$$E_H=2a\left[\frac{C_{11}-C_{12}}{C_{11}}\right]\epsilon_{\parallel} , \tag{7a}$$

$$E_U=-b\left[\frac{C_{11}+2C_{12}}{C_{11}}\right]\epsilon_{\parallel} . \tag{7b}$$

a and b are the hydrostatic and shear deformation potentials, respectively. The matrix elements derived from the strain Hamiltonian (6) leaves the HH band uncoupled to the other bands, but the coupling of the LH and SO bands occurs by the matrix element of $\sqrt{2}E_U$.[12] It will be discussed in Sec. V that the decoupling of the LH and SO bands is a reasonable approximation for a relatively large spin-orbit split-off energy of GaAs and InAs. Then the remaining strain terms are diagonalized and the matrix elements of $(-E_H-E_U)$ and $(-E_H+E_U)$ are added in the diagonal terms of $\langle\frac{3}{2},\pm\frac{3}{2}|\frac{3}{2},\pm\frac{3}{2}\rangle$ and $\langle\frac{3}{2},\pm\frac{1}{2}|\frac{3}{2},\pm\frac{1}{2}\rangle$, respectively.

A unitary transformation following the method of Broido and Sham[13] block diagonalizes the above 4×4 Hamiltonian into the two 2×2 Hamiltonians. One of them is given by

$$[\bar{H}]=\begin{bmatrix} F-E_H-E_U & K^* \\ K & G-E_H+E_U \end{bmatrix}, \tag{8}$$

where

$$K=\left[-\frac{\hbar^2}{2m_0}\right]\sqrt{3}k^2(\eta\sin^2\theta+i\gamma_3\sin2\theta) , \tag{9}$$

$$\eta=[\gamma_2^2\cos^2(2\phi)+\gamma_3^2\sin^2(2\phi)]^{1/2} . \tag{10}$$

The angles θ and ϕ are defined to give $k_z=k\cos\theta$, $k_t=k\sin\theta$, $k_y=k_t\sin\phi$, and $k_x=k_t\cos\phi$. The other Hamiltonian is given by the exchange of the nondiagonal terms in Eq. (8). The corresponding basis set is given by

$$\begin{aligned} |u_{\pm3/2}\rangle&=(1/\sqrt{2})(e^{-i\xi_+}|u_1\rangle\pm e^{i\xi_+}|u_4\rangle) , \\ |u_{\pm1/2}\rangle&=(1/\sqrt{2})(\pm e^{i\xi_-}|u_2\rangle+e^{-i\xi_-}|u_3\rangle) , \end{aligned} \tag{11}$$

where the basis set with the upper sign corresponds to the Hamiltonian in Eq. (8) and

$$\xi_\pm=\frac{\pi}{4}+\frac{\phi}{2}\pm\tfrac{1}{2}\tan^{-1}\left[\frac{\gamma_3}{2\gamma_2}\tan(2\phi)\right] . \tag{12}$$

These two 2×2 Hamiltonians are doubly degenerate.

For the treatment of the QW valence band, the potential term

$$V(z)=\begin{cases} 0, & |z\le L_z/2 \\ V_0, & |z|>L_z/2 \end{cases} \tag{13}$$

must be included in the eigenvalue problem, that is,

$$|\bar{H}+V(z)I-EI|=0 . \tag{14}$$

When this equation is solved in the well and barrier regions, the E-$\mathbf{k}$ (k_x,k_y,k_z) relation in the respective region is obtained. For a given energy value E and the wave numbers of k_x and k_y in the QW plane, the two pairs of the solutions for k_z which are complex conjugate to each other are obtained. When the basis functions in Eq. (11) are expressed in a general form of φ_n, the wave function corresponding to the one of the solution k_{zm} is given by

$$\psi_{k_{zm}}(z)=\sum_n e^{ik_{zm}z}B_n(k_{zm})\varphi_n , \tag{15}$$

where the relative amplitude $B_n(k_{zm})$ is solved from the

simultaneous equations corresponding to Eq. (14). The term $e^{i\mathbf{k}_t\cdot\mathbf{r}}$ is omitted in Eq. (15) and in the following expressions. The wave function in general is given by the superposition of Eq. (15) for the four k_{zm} solutions:

$$\psi(z)=\sum_m a_m \psi_{k_{zm}}(z) . \tag{16}$$

The amplitudes a_m are to be determined from the boundary conditions shown below.

In the case of the multiband theory, the boundary conditions at a heterointerface are given by the continuity of the probability current.[14] As will be shown below, the strain terms do not appear in the boundary conditions explicitly except for the modification of the band offset.[15] In the present case, the probability current normal to the heterointerface is given by

$$J_z=-\frac{1}{i\hbar}\int[\psi^*(z)H\psi(z)-\psi(z)H\psi^*(z)]dz . \tag{17}$$

The integral is assumed to be taken in a thin layer of a unit area at the interface. When Eq. (15) is substituted into Eq. (16), the wave function is also expressed as

$$\psi(z)=\sum_n F_n(z)\varphi_n , \tag{18a}$$

$$F_n(z)=\sum_m a_m e^{ik_{zm}z}B_n(k_{zm}) . \tag{18b}$$

When the integral in each unit cell of the basis function φ_n is performed in Eq. (17), the integral reduces to

$$\int\psi^*(z)H\psi(z)dz=\sum_{jj'}\int F_j^*(z)D_{jj'}F_{j'}(z)dz , \tag{19}$$

where $D_{jj'}$ is the matrix elements given in Eq. (8) expressed in the following general form:

$$D_{jj'}=D_{jj'}^{\alpha\beta}k_\alpha k_\beta+\delta E_{jj'} . \tag{20}$$

$\delta E_{jj'}$ is the strain jj' matrix term given in Eq. (8). To evaluate the remaining integral on the envelope functions in Eq. (19), k_z in Eq. (20) [or in Eq. (8)] is replaced with $-i\partial/\partial z$. After the integration along the z direction in an infinitesimal region near the interface, the terms which do not have the $\partial/\partial z$ term all vanish. The probability current in the z direction is then given by

$$J_z=2\,\mathrm{Re}\left[\frac{1}{\hbar}\sum_j F_j^*(z)\sum_{j'}\left[D_{jj'}^{\alpha z}+D_{jj'}^{z\beta}-iD_{jj'}^{zz}\frac{\partial}{\partial z}\right]F_{j'}(z)\right] , \tag{21}$$

which does not include the strain terms. Another condition is given by the continuity of the wave function (18a). When the basis function φ_n is similar across the heterointerface, it reduces to the continuity of the envelope function $F_j(z)$ using the orthogonality of the basis functions. The mismatch of the basis function across the interface will be discussed in Sec. V. Using this condition, the continuity of Eq. (21) is satisfied by the additional continuity condition of the terms summed over j' in the same equation. Then the boundary conditions in the present case are given by the continuity of the following equations across the interface:

$$F_{3/2}(z) \text{ and } F_{1/2}(z) , \tag{22a}$$

$$\left[-i(\gamma_1-2\gamma_2)\frac{\partial}{\partial z}F_{3/2}(z)+i2\sqrt{3}\gamma_3 k_t F_{1/2}(z)\right] , \tag{22b}$$

$$\left[-i2\sqrt{3}\gamma_3 k_t F_{3/2}(z)-i(\gamma_1+2\gamma_2)\frac{\partial}{\partial z}F_{1/2}(z)\right] . \tag{22c}$$

The boundary conditions given in Eq. (22) give the eight conditions at the two heterointerfaces at $z=\pm L_z/2$ of a QW. The number of the amplitude coefficients a_m to be determined is four in the well region and two for the respective barrier region considering that the wave functions are infinitesimal at infinity z. This gives the eight equations for the eight amplitude coefficients a_m to be determined. By solving the resultant 8×8 determinant, the valence-subband structure is numerically obtained.

III. ANALYTICAL EXPRESSION FOR A BAND-EDGE HOLE MASS

The above equations can be solved only with a numerical method. When an infinite barrier is assumed, an analytical expression for the effective mass at the zone center can be derived as shown in the following. The boundary conditions at the heterointerface in this case are simply given by

$$F_{3/2}(\pm L_z/2)=0 \text{ and } F_{1/2}(\pm L_z/2)=0 . \tag{23}$$

Then the above 8×8 determinant resulting from the boundary conditions (22) is reduced to the 4×4 determinant from which the following equation is derived:

$$8\gamma_3^2\Delta_1(k_+)\Delta_1(k_-)k_+k_-[1-\cos(k_+L_z)\cos(k_-L_z)]$$
$$=\{\eta^2[\Delta_1(k_+)-\Delta_1(k_-)]^2k_t^2+4\gamma_3^2[\Delta_1^2(k_+)k_-^2+\Delta_1^2(k_-)k_+^2]\}\sin(k_+L_z)\sin(k_-L_z) , \tag{24}$$

where

$$\Delta_1(k_\pm)=G(k_\pm)-E_H+E_U-E . \tag{25}$$

The following equation is also obtained from Eq. (14) in the well region:

$$E^2-(F+G-2E_H)E$$
$$+(F-E_H-E_U)(G-E_H+E_U)-|K|^2=0 . \tag{26}$$

Substitution of $k_t=0$ in Eqs. (24) and (26) yields

$$k_{\pm}L_z|_{k_t=0}=n_{\pm}\pi, \quad n_{\pm}=1,2,\ldots, \tag{27}$$

where k_+ and k_- are the solutions of k_z obtained from Eq. (26) for a given energy value E. Taking the first derivatives of Eqs. (24) and (26) with respect to k_t, the following relation is obtained by using Eq. (27):

$$\left.\frac{\partial k_{\pm}}{\partial k_t}\right|_{k_t=0}=0 . \tag{28}$$

The hole mass at the zone center, which is defined by

$$m_{vt}=-\hbar^2\left[\left.\frac{\partial^2 E}{\partial k_t^2}\right|_{k_t=0}\right]^{-1}, \tag{29}$$

is obtained by taking the second derivatives of Eqs. (24) and (26) with respect to k_t and by using the relations (27) and (28). The derived final expression for the hole mass is the following:

$$\left[\frac{m_{vt}}{m_0}\right]^{-1}=\gamma_1\pm\left[\gamma_2-\frac{3\gamma_3^2}{\gamma_2+\delta\gamma_{a\mp}}\right]+3[\gamma_1\mp(2\gamma_2+4\delta\gamma_{a\mp})]\left[\frac{\gamma_3}{\gamma_2+\delta\gamma_{a\mp}}\right]^2\times\frac{(-1)^{n_{\mp}+1}+\cos(k_{\pm}L_z)}{(k_{\pm}L_z)\sin(k_{\pm}L_z)} , \tag{30a}$$

where

$$k_{\pm}L_z=\{[\gamma_1\mp(2\gamma_2+4\delta\gamma_{a\mp})]/(\gamma_1\pm 2\gamma_2)\}^{1/2}(n_{\mp}\pi) , \tag{30b}$$

$$\delta\gamma_{a\pm}=2E_U\Big/\left[\frac{\hbar^2}{2m_0}\left[\frac{2n_{\pm}\pi}{L_z}\right]^2\right] . \tag{30c}$$

In this equation, the upper sign corresponds to the HH subband and the lower sign corresponds to the LH subband. As is clearly seen in Eq. (30), the derived hole mass is independent of the crystalline direction in the (001) QW plane and is isotropic even if the band warping is taken into account. Without strain, Eq. (30) is reduced to[4]

$$\left[\frac{m_{vt}}{m_0}\right]^{-1}=\gamma_1+\gamma_2-\frac{3\gamma_3^2}{\gamma_2}+3(\gamma_1-2\gamma_2)\left[\frac{\gamma_3}{\gamma_2}\right]^2\times\frac{(-1)^{n_-+1}+\cos(k_+L_z)}{(k_+L_z)\sin(k_+L_z)} , \tag{31a}$$

$$k_+L_z=[(\gamma_1-2\gamma_2)/(\gamma_1+2\gamma_2)]^{1/2}(n_-\pi) \tag{31b}$$

for the HH subband hole mass. When the isotropy is assumed such that $\gamma_2=\gamma_3$, Eq. (31a) is simplified further and is reduced to the expression derived by Fasolino and Altarelli:[16]

$$\left[\frac{m_{vt}}{m_0}\right]^{-1}=(\gamma_1-2\gamma_2)\left[1+3\frac{(-1)^{n_-+1}+\cos(k_+L_z)}{(k_+L_z)\sin(k_+L_z)}\right] . \tag{32}$$

The above expressions give the hole mass modified from the bulk mass values. This is interpreted from the following simple model. When the bulk hole mass is given by m^*, the hole kinetic energy is given by

$$E=-\frac{\hbar^2}{2m^*}(k_t^2+k_z^2) . \tag{33}$$

The corresponding hole mass defined by Eq. (29) is given by

$$(m_{vt})^{-1}=\frac{1}{m^*}\left[1+\left[\frac{\partial k_z}{\partial k_t}\right]^2+k_z\frac{\partial^2 k_z}{\partial k_t^2}\right]\Bigg|_{k_t=0} . \tag{34}$$

Equation (28) indicates that the second term in Eq. (34) is zero. The third term, on the other hand, is finite even for the infinite barrier, since the boundary conditions in Eq. (23) are satisfied by the superposed envelope functions given by Eq. (18b), and the k_z value defined by Eq. (27) at the zone center is allowed to be changed for the finite k_t value. The direct correspondence of Eq. (34) to Eq. (32) will be evident.

IV. NUMERICAL RESULTS

The band-edge hole mass in a strained QW is evaluated in this section. Numerical calculations were performed on an $In_xGa_{1-x}As$ alloy, which was studied extensively recently for strained-QW lasers. The material parameters used for the calculations are listed in Tables I and II.

First, the hole mass at the zone center was evaluated with the analytical expression given in Eq. (30). A 100-Å $In_xGa_{1-x}As$ QW with the $In_{0.52}Al_{0.48}As$ barrier lattice matched to InP was assumed. The results are shown in Fig. 1 by the solid line indicated as the analytical model with strain. The $In_xGa_{1-x}As$ QW is lattice matched to InP with the x value of 0.53 and is under in-plane compression for the larger x value. The in-plane compressive strain is 0.82% for $x=0.65$ and is increased to 3.14% for $x=1.0$. For the purpose of illustrating the strain effect on the mass value, the mass value was calculated without strain by the analytical expression in Eq. (31). A comparison of the two analytical models indicates that the in-plane compression slightly reduces the mass value.

TABLE I. Energy gap (E_g), spin-orbit split-off energy (Δ), hydrostatic (a) and shear (b) deformation potentials are in eV, and elastic constants C_{11} and C_{12} are in 10^{11} dyn/cm^2.

	E_g	Δ	a	b	C_{11}	C_{12}
GaAs	1.424	0.34	−8.9[a]	−1.73	11.88	5.38
InAs	0.356	0.38	−6.0[b]	−1.2	8.33	4.53

[a]Reference 17.
[b]Reference 18.

TABLE II. Luttinger mass parameters and lattice constants.

	γ_1	γ_2	γ_3	Lattice constants (Å)
GaAs	6.85[a]	2.10	2.90	5.6537
InAs	19.67[b]	8.37	9.29	6.058
AlAs	4.04[b]	0.78	1.57	5.6611

[a]Reference 19.
[b]Reference 20.

As described in the preceding section, the analytical expressions for the band-edge hole mass were derived assuming the infinite-barrier height and this assumption usually gives the larger subband energy. For the purpose of studying the effect of the finite-barrier height on the band structure as well as on the band-edge hole mass, the results calculated with the assumption of the infinite-barrier height will be compared with those calculated by taking into account the boundary conditions correctly at the heterointerface. Therefore the effective well width[21] was used in the analytical model so that the subband energy calculated with the assumption of the infinite-barrier height would give the same energy level as the one calculated considering the finite-barrier height. Since accurate data on the band offset are not available at present in this strained system, the valence-band offset was tentatively assumed to be 40% of ΔE_g, which is the same as that for the $GaAs/Al_xGa_{1-x}As$ system.[22] Then the effective well width calculated for the lowest valence subband of the 100-Å $In_xGa_{1-x}As$ QW shown in Fig. 1 is 111.8 Å for $x=0.65$ and is slightly reduced to 110.4 Å for $x=1.0$. The mass values estimated with the analytical models shown in Fig. 1 were calculated with these effective well widths. In the absence of the strain, the mass value is independent of the well width, as is clearly seen in Eq. (31). Even with the presence of strain, the modification of the mass value with the introduction of the effective well width in Eq. (30) is less than 1% in comparison to the value calculated with the actual well width.

The mass values calculated with the above analytical models were compared with the one calculated numerically by taking the boundary conditions into account at the heterointerface following the method described in Sec. II (the latter will hereafter be called the "finite-barrier model"). The finite-barrier model, shown as the upper solid line in Fig. 1, has a slightly larger hole mass than the analytical models due to the field penetration into the barrier region. The tendency for the larger difference between the finite-barrier model and the analytical models for the smaller In mole fraction in Fig. 1 is due to the reduction of the valence-band offset.

The effect of the finite-barrier height on the whole valence-subband structure is shown in Fig. 2. A 50-Å $In_{0.9}Ga_{0.1}As$ QW with the $In_{0.52}Al_{0.48}As$ barrier lattice matched to InP, where the QW is under 2.6% biaxial compression, was assumed in this case. The valence-band offset was also assumed to be 40% of the ΔE_g. The solid line is the band structure calculated by taking the finite-barrier height into account at the heterointerface. The dashed line is the band structure calculated assuming the infinite-barrier height where the effective well width of 60.5 Å was used to give the same subband energies as those calculated with the finite-barrier model. The difference between the two curves indicates the increase of the band-edge hole mass shown in Fig. 1 as well as the increase of the subband nonparabolicity in the higher-energy region due to the penetration of the wave functions into the barrier region.

Figure 3 shows the calculated well-width dependence of the band-edge hole mass for an $InAs/In_{0.52}Al_{0.48}As$ QW to illustrate the influence of the field penetration into the barrier region. It will be clear from Fig. 3 that the analytical model predicts a weak well-width dependence of the mass value, the change of which is within 4% in the range of the well width shown in Fig. 3. The effective

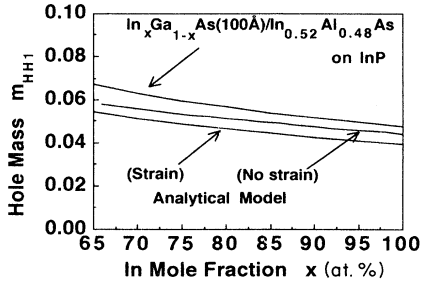

FIG. 1. The band-edge hole mass estimated for a 100-Å $In_xGa_{1-x}As$ QW with the $In_{0.52}Al_{0.48}As$ barrier lattice matched to InP. The upper curve was obtained from the band structure near the zone center calculated numerically with the correct treatment of the boundary conditions following the procedure described in Sec. II. The analytical models with and without strain were calculated with the analytical expression in Eqs. (30) and (31), respectively. The effective well width, which is about 10 Å larger than the actual well width, was used in these analytical models.

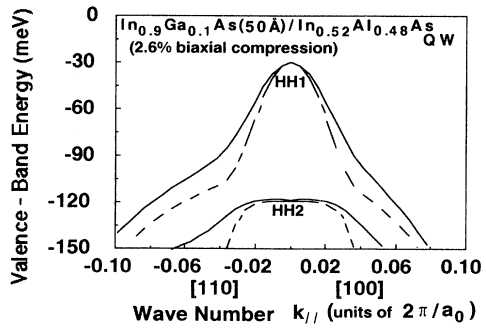

FIG. 2. Comparison of the subband structures calculated by taking the finite-barrier height into account (solid line) and with the infinite-barrier approximation (dashed line). A 50-Å $In_{0.9}Ga_{0.1}As$ QW under 2.6% biaxial compression was assumed. The effective well width of 60.5 Å was used in the infinite-barrier model.

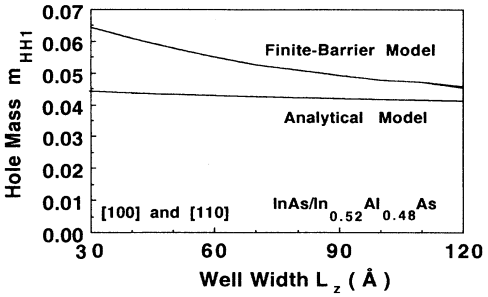

FIG. 3. Well-width dependence of the hole mass at the top of the valence band evaluated with the finite-barrier model and with the analytical model given by Eq. (30). The hole masses estimated with the finite-barrier model using the subband dispersions in the [100] and [110] directions are indistinguishable due to the isotropy of the mass values at the band edge as indicated by Eq. (30). The hole mass estimated with the finite-barrier model increases for the smaller well width due to the penetration of the wave function into the barrier region.

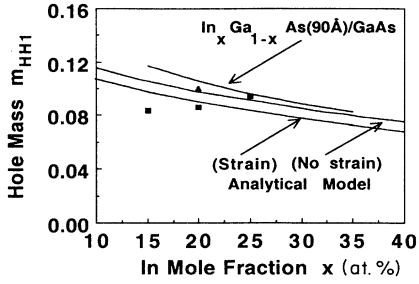

FIG. 4. Comparison of the measured hole masses with the theoretical calculations. The solid squares and triangle are the measured hole mass values in Refs. 23 and 24, respectively. The upper solid curve was calculated for a 90-Å $In_xGa_{1-x}As$ QW considering the boundary conditions with the GaAs barriers. The analytical models with and without strain were calculated from Eqs. (30) and (31), respectively.

well width used in the calculation of the analytical model is about 10 Å larger than the actual well width given in Fig. 3, but this effect is small. In the finite-barrier model, where the boundary conditions at the heterointerface were correctly taken into account, the hole mass was evaluated using the subband dispersion curves numerically calculated in the [100] and [110] directions. But the orientation dependence of the estimated hole mass is indistinguishable in Fig. 3. This isotropic property of the band-edge hole mass numerically evaluated with the finite-barrier model is consistent with the isotropy predicted by the analytical model given in Eq. (30). The absolute mass value, however, is considerably increased for the smaller well width due to the penetration of the wave function into the barrier region. Therefore the application of the analytical expression (30) to estimate the hole mass at the top of the valence band is a reasonable approximation for a relatively wide well width.

There have been several reports on the measurements of the hole mass in strained-QW structures. They are mostly on $In_xGa_{1-x}As/GaAs$ structures. The measured mass values are shown in Fig. 4.[23,24] The upper solid curve was calculated with the finite-barrier model on a 90-Å $In_xGa_{1-x}As$ QW taking into account the boundary conditions at the heterointerfaces. The band offset in this material system is still controversial and the valence-band offset for the In mole fraction below 20% changes from 20% to 60% of the ΔE_g.[25] For the In mole fraction of 20~40 %, on the other hand, the valence-band offset of 20% seems to be reliable[25] and this band offset was assumed in Fig. 4. The in-plane compressive strain in the $In_xGa_{1-x}As$ QW ranges from 1.06% for $x=0.15$ to 2.44% for $x=0.35$. The analytical models with and without strain were calculated with Eqs. (30) and (31), respectively, using the effective well width ranging from 129.3 Å for $x=0.15$ to 116.3 Å for $x=0.35$. The agreement between the theory and the measurements is not necessarily satisfactory at present, but at least the significant reduction of the hole mass will be evident theoretically and experimentally compared with the bulk HH mass ranging from 0.446 to 0.434 for the In mole fraction shown in Fig. 4.

V. DISCUSSIONS

On the treatment of the strain Hamiltonian given in Eq. (6), the coupling of the LH and SO bands by the matrix element of $\sqrt{2}E_U$ was indicated. E_U is the shear deformation-potential term given in Eq. (7b), which is proportional to the in-plane strain $\epsilon_{\|}$. Therefore this term will become larger for the larger strain. The contribution of this term was examined by the strain dependence of the bulk band edge at the zone center. At $k_t=0$, the 8×8 Hamiltonian including the strain terms reduces to the doubly degenerate 4×4 matrix. The C band in this matrix is decoupled and the following equations for the valence bands result from the eigenequation:[12]

$$E=-E_H-E_U\ , \tag{35a}$$

$$E=-E_H-\tfrac{1}{2}[(\Delta-E_U)\mp(9E_U^2+2E_U\Delta+\Delta^2)^{1/2}]\ , \tag{35b}$$

where Δ is the spin-orbit split-off energy. The energy was measured from the valence-band top at zero strain. Equation (35a) corresponds to the HH band. The upper and lower signs in Eq. (35b) correspond to the LH and SO bands, respectively. For $\Delta\gg E_U$, the equation for the LH band reduces to

$$E=-E_H+E_U\ , \tag{36}$$

which corresponds to the diagonal term in Eq. (8) for $k=0$. The solid lines in Fig. 5 are the strain dependence of the valence-band edges calculated from Eqs. (35) for InAs. 0.38 eV was used for the Δ value. The dashed line is the strain dependence of the LH band calculated with the approximation of Eq. (36). The difference between the two curves for the LH band is the indication of the coupling of the LH-SO band and is very small up to 1% of the strain. For the larger strain, the LH subband will be modified to some extent by this coupling effect. How-

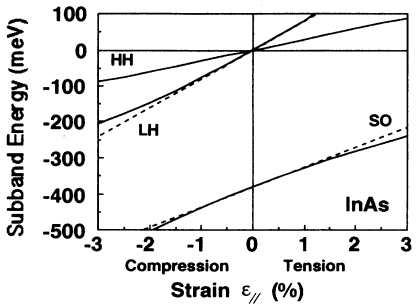

FIG. 5. Strain dependence of the bulk valence-band edges calculated with the LH-SO band coupling (solid lines) and without the coupling (dashed lines for LH and SO bands) in InAs.

ever, the HH1 subband, which gives the valence-band edge under the in-plane compression, is not much influenced by this effect near the zone center. The HH1 subband near the zone center is the pure HH band and the band-edge hole mass derived in Sec. III will not be modified by this coupling even for the larger strain. However, the subband nonparabolicity for the larger k_t value, where the band mixing is significant, will be more affected due to the LH band mixing. Similar examination was performed on GaAs. The influence of this coupling term was similar to that in InAs, and a similar argument is applicable for an $In_xGa_{1-x}As$ alloy.

In the treatment of the boundary conditions in Sec. II, the continuity of the envelope functions given in Eq. (22a) was derived by assuming the common basis function across the heterointerface. Eppenga, Schuurmans, and Colak[7] discussed the mismatch effect of the basis functions in detail. They compared the effective-mass theory similar to the present method with the nearest-neighbor tight-binding approach by calculating the subband energies and the subband structures of a $GaAs/Al_xGa_{1-x}As$ QW. They indicated close agreement of the two methods, and a small mismatch of the basis functions, at least in the case of the $GaAs/Al_xGa_{1-x}As$ system. As for the other material systems treated in this paper, a similar detailed discussion is not available at present. But as long as the characteristics calculated with the finite-barrier model are close to the infinite-barrier model, the description of the subband structure near the zone center will remain valid quantitatively.

An analytical expression for a band-edge hole mass was previously derived for a uniaxial stress parallel to [100] in the (001) QW plane.[26] The resultant equation is similar to Eq. (30) but slightly different. The indication of Eq. (30) in the present paper is that the hole mass at the zone center is isotropic even if the warping of the valence band is taken into account. This isotropy of the band-edge hole mass and the reduced subband nonparabolicity in the strained-QW structures relative to the lattice-matched QW's were reflected as significant improvements in the calculated laser properties.[4]

VI. SUMMARY

The analytical expression was derived for the hole mass at the top of the valence band and this indicated that the mass value is isotropic even if the warping of the valence band and the biaxial stress are taken into account. This was also confirmed by the numerical calculations following the procedure given in Sec. II, where the boundary conditions at the heterointerface are correctly taken into account. Under the in-plane compressive stress in the (001) QW plane, the valence-band edge is given by the band designated by $|J,m_J\rangle=|\frac{3}{2},\pm\frac{3}{2}\rangle$, which corresponds to the bulk HH band, and the estimated mass values showed weak strain dependence. The effect of the finite-barrier height on the mass value was also discussed.

The calculated hole masses were close to the mass values measured in strained QW's. Although the quantitative agreement was not necessarily satisfactory at present, the significant reduction of the hole mass compared with the bulk mass was demonstrated theoretically and experimentally.

[1]Y. C. Chang, Appl. Phys. Lett. **46**, 710 (1985).
[2]E. Yablonovitch and E. O. Kane, IEEE J. Lightwave Technol. **LT-4**, 961 (1986).
[3]A. R. Adams, Electron. Lett. **22**, 249 (1986).
[4]I. Suemune, L. A. Coldren, M. Yamanishi, and Y. Kan, Appl. Phys. Lett. **53**, 1378 (1988).
[5]T. Ohtoshi and N. Chinone, IEEE Photon. Technol. Lett. **1**, 117 (1989).
[6]J. M. Luttinger and W. Kohn, Phys. Rev. **97**, 869 (1955).
[7]R. Eppenga, M. F. H. Schuurmans, and S. Colak, Phys. Rev. B **36**, 1554 (1987).
[8]E. O. Kane, J. Phys. Chem. Solids **1**, 249 (1957).
[9]V. A. Chitta, M. H. Degani, and A. M. Cohen, Phys. Rev. B **38**, 8533 (1988).
[10]D. S. Citrin and Y. C. Chang, Phys. Rev. B **40**, 5507 (1989).
[11]G. E. Pikus and G. L. Bir, Fiz. Tverd. Tela (Leningrad) **1**, 1642 (1959) [Sov. Phys.—Solid State **1**, 1502 (1959)].
[12]F. H. Pollak and M. Cardona, Phys. Rev. **172**, 816 (1968).
[13]D. A. Broido and L. J. Sham, Phys. Rev. B **31**, 888 (1985).
[14]M. Altarelli, Phys. Rev. B **28**, 842 (1983).
[15]C. G. Van de Walle and R. M. Martin, Phys. Rev. B **35**, 8154 (1987).
[16]A. Fasolino and M. Altarelli, *Two Dimensional Systems, Heterostructures and Superlattices,* edited by G. Bauer, F. Kuchar, and H. Heinrich (Springer, Berlin, 1984), p. 176.
[17]M. Chandrasekhar and F. H. Pollak, Phys. Rev. B **15**, 2127 (1977).
[18]*Landolt-Börnstein, Numerical Data and Functional Relationships in Science and Technology,* edited by O. Madelung (Springer, Berlin, 1982), Vol. 17, Group III.
[19]G. D. Sanders and Y. C. Chang, Phys. Rev. B **35**, 1300 (1987).
[20]P. Lawaetz, Phys. Rev. B **4**, 3460 (1971).
[21]D. A. B. Miller, D. S. Chemla, T. C. Damen, A. C. Gossard, W. Wiegmann, T. H. Wood, and C. A. Burrus, Phys. Rev. B

32, 1043 (1985).
[22]R. C. Miller, D. A. Kleinman, and A. C. Gossard, Phys. Rev. B **29**, 7085 (1984).
[23]E. D. Jones, S. K. Lyo, I. J. Fritz, J. F. Klem, J. E. Schirber, C. P. Tigges, and T. J. Drummond, Appl. Phys. Lett. **54**, 2227 (1989).
[24]I. J. Fritz, J. E. Schirber, E. D. Jones, T. J. Drummond, and G. C. Osbourn, in IOP Conf. Proc. No. 83 (Institute of Physics, Bristol, 1986), p. 233.
[25]M. J. Joyce, M. J. Johnson, M. Gal, and B. F. Usher, Phys. Rev. B **38**, 10 978 (1988).
[26]J. Lee and M. O. Vassell, Phys. Rev. B **37**, 8855 (1988).